Current Biology, Volume *32*

Supplemental Information

Olfactory stimuli and moonwalker SEZ neurons can drive backward locomotion in *Drosophila*

Shai Israel, Eyal Rozenfeld, Denise Weber, Wolf Huetteroth, and Moshe Parnas

Figure S1

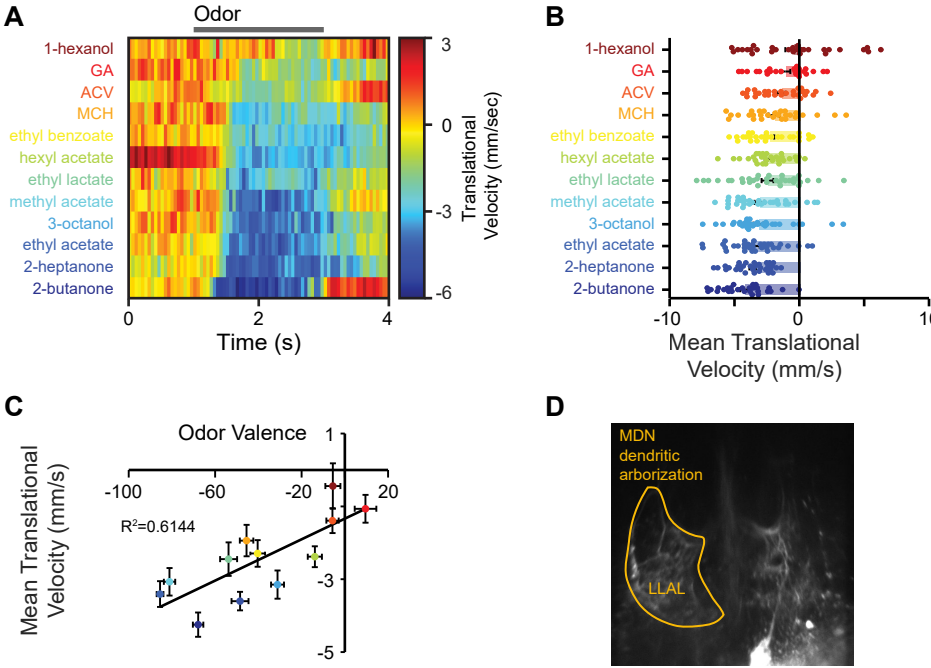
A
Odor
1-hexanol
GA
ACV
MCH
ethyl benzoate
hexyl acetate
ethyl lactate
methyl acetate
3-octanol
ethyl acetate
2-heptanone
2-butanone
0
2
4
Time (s)
3
0
-3
-6
Translational Velocity (mm/sec)
B
-10
0
10
Mean Translational Velocity (mm/s)
C
Odor Valence
-100
-60
-20
20
1
-3
-5
R²=0.6144
Mean Translational Velocity (mm/s)
D
MDN dendritic arborization
LLAL

Figure S1: Odor-evoked backward locomotion in linear chambers. Related to Figure 1

(**A**) Translational velocity matrix of w^{1118} flies following application of different odors in the linear chambers. The data during the two second odor pulse (horizontal grey line) is flanked by one second before and after odor application. GA stands for geranyl acetate, ACV stands for Apple Cider Vinegar, and MCH stands for 4-methylcyclohexanol.

(**B**) Mean translational velocity during the two second odor pulse obtained from traces used to compose the matrix in (A). A clear backward locomotion response is observed only for some of the delivered odors ($25 \leq n \leq 34$).

(**C**) Mean translational velocity plotted against odor valence. Backward walking correlates with odor valence as aversive odors induce stronger backward locomotion than appetitive odors ($R^2 = 0.6144$). Odor valence values were obtained from[S1].

(**D**) Representative region of interest (ROI), labeled with orange polygon, used for Ca^{2+} imaging of odor-evoked responses in MDN dendritic arbors in an example projection image. The ROI was located in the lower lateral accessory lobe (LLAL).

Figure S2

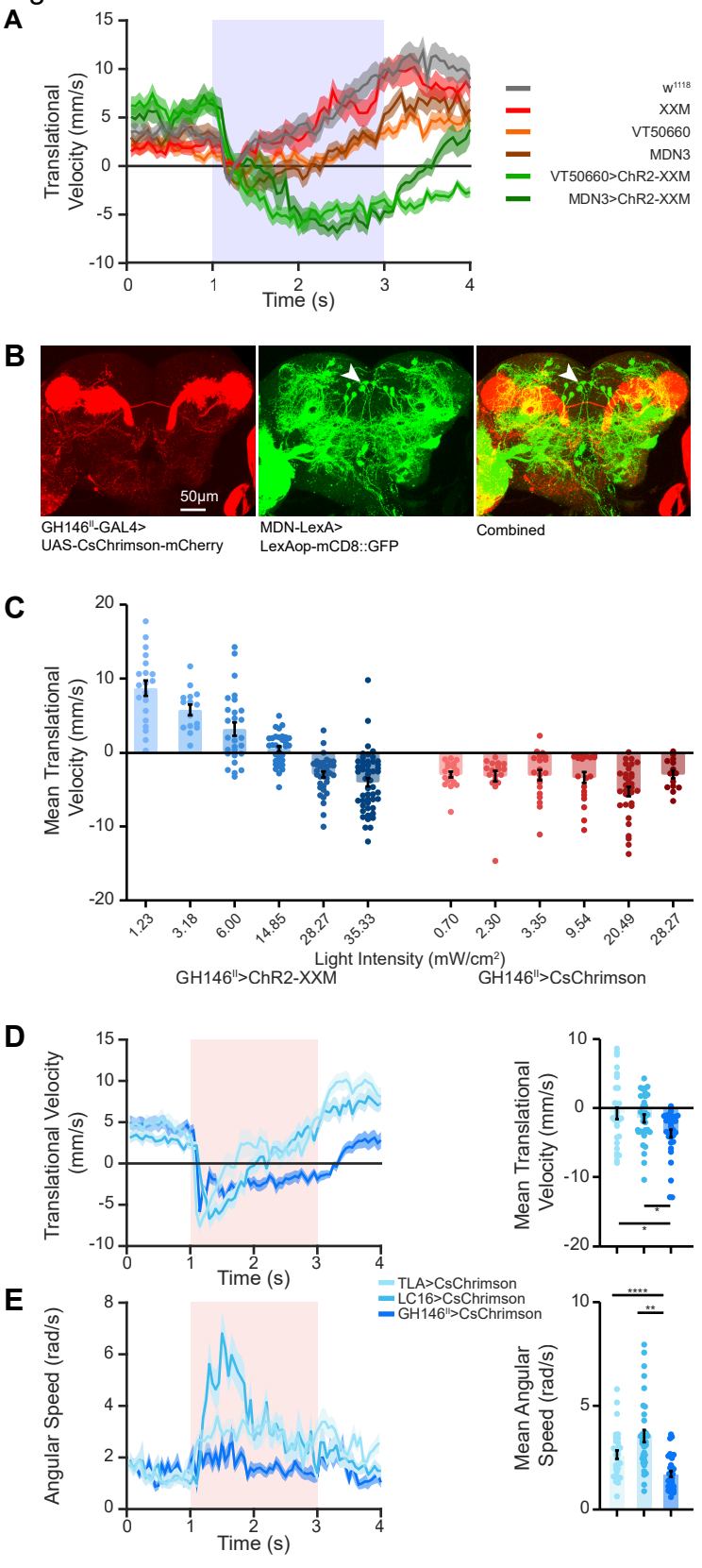
A
Translational Velocity (mm/s)
Time (s)
w1118
XXM
VT50660
MDN3
VT50660>ChR2-XXM
MDN3>ChR2-XXM
B
50μm
GH146II-GAL4>
UAS-CsChrimson-mCherry
MDN-LexA>
LexAop-mCD8::GFP
Combined
C
Mean Translational Velocity (mm/s)
1.23
3.18
6.00
14.85
28.27
35.33
0.70
2.30
3.35
9.54
20.49
28.27
Light Intensity (mW/cm2)
GH146II>ChR2-XXM
GH146II>CsChrimson
D
Translational Velocity (mm/s)
Time (s)
Mean Translational Velocity (mm/s)
E
TLA>CsChrimson
LC16>CsChrimson
GH146II>CsChrimson
Angular Speed (rad/s)
Time (s)
Mean Angular Speed (rad/s)

Figure S2: Characterization of GH146^{II}-GAL4 mediated backward locomotion. Related to Figure 2

(**A)** Translational velocity ± SEM (shading) over time in the open arena. Genotypes as designated. Optogenetic stimulation activating ChR2-XXM was given between one and three seconds. Light pulse is labeled in light blue.

(**B**) GH146^{II}-GAL4 was used to drive CsChrimson-mCherry (left). MDNs were labeled using VT44845-LexA driving GFP (middle). White arrowheads mark MDN cell bodies. No overlap is observed between GH146^{II}-GAL4 labeled neurons and MDNs (right). Maximum intensity projections of 100 confocal sections (1 µm) through the central brain are presented.

(**C**) Effects of light intensity on optogenetic-induced backward locomotion in the open arena. GH146^{II}-GAL4 was used to drive either UAS-CsChrimson or UAS-ChR2-XXM. The mean translational velocity during a two second blue (ChR2-XXM) or red (CsChrimson) light pulse obtained for different light intensities is presented.

(**D and E**) *Left,* Translational velocity (D) and angular speed (E) ± SEM (shading) elicited by activation of visual projection neurons (LC16-1-GAL4), TwoLumps Ascending neurons (TLA-GAL4) or GH146^{II}-GAL4 driving UAS-CsChrimson in the open arena. Sustained and straight backward walking is observed only for GH146^{II}-GAL4 driver line following a two second red light pulse. The two second light pulse is labeled in light red. *Right*, mean translational velocity (D) and mean angular speed (E) during the two second light pulse obtained from traces on the left. Activation of TLA and LC16 neurons led to significantly lower translational velocity and increased angular speed ($31 \leq n \leq 34$, * $p < 0.05$, ** $p < 0.01$, **** $p < 0.0001$, Kruskal - Wallis tests followed by Dunn's post-hoc tests).

Figure S3

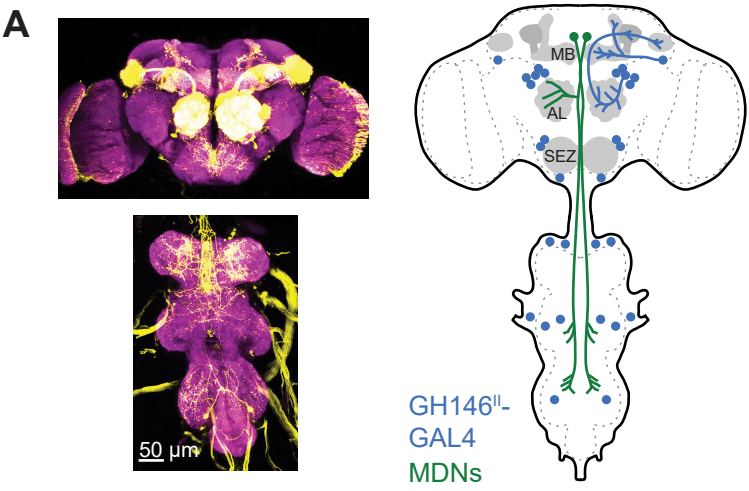
A
50 µm
MB
AL
SEZ
GH146II-
GAL4
MDNs
B
50 µm
MB
AL
SEZ
NP225-
GAL4
MDNs
C
50 µm
MB
AL
SEZ
NP5288-
GAL4
MDNs

Figure S3: GH146^{II}-, NP225- and NP5288-GAL4 anatomy. Related to Figure 4

(**A, B and C**) *Left*, Expression pattern of GH146^{II}-GAL4 (A), NP225-GAL4 (B), and NP5288-GAL4 (C). UAS-CsChrimson.mVenus was used to label the cells. Maximum intensity projections of 150 confocal sections (1 µm) through the central brain and VNC are presented. *Right*, Schematic drawings of the expression pattern of the driver lines on the left (blue) and of MDNs (green).

Figure S4

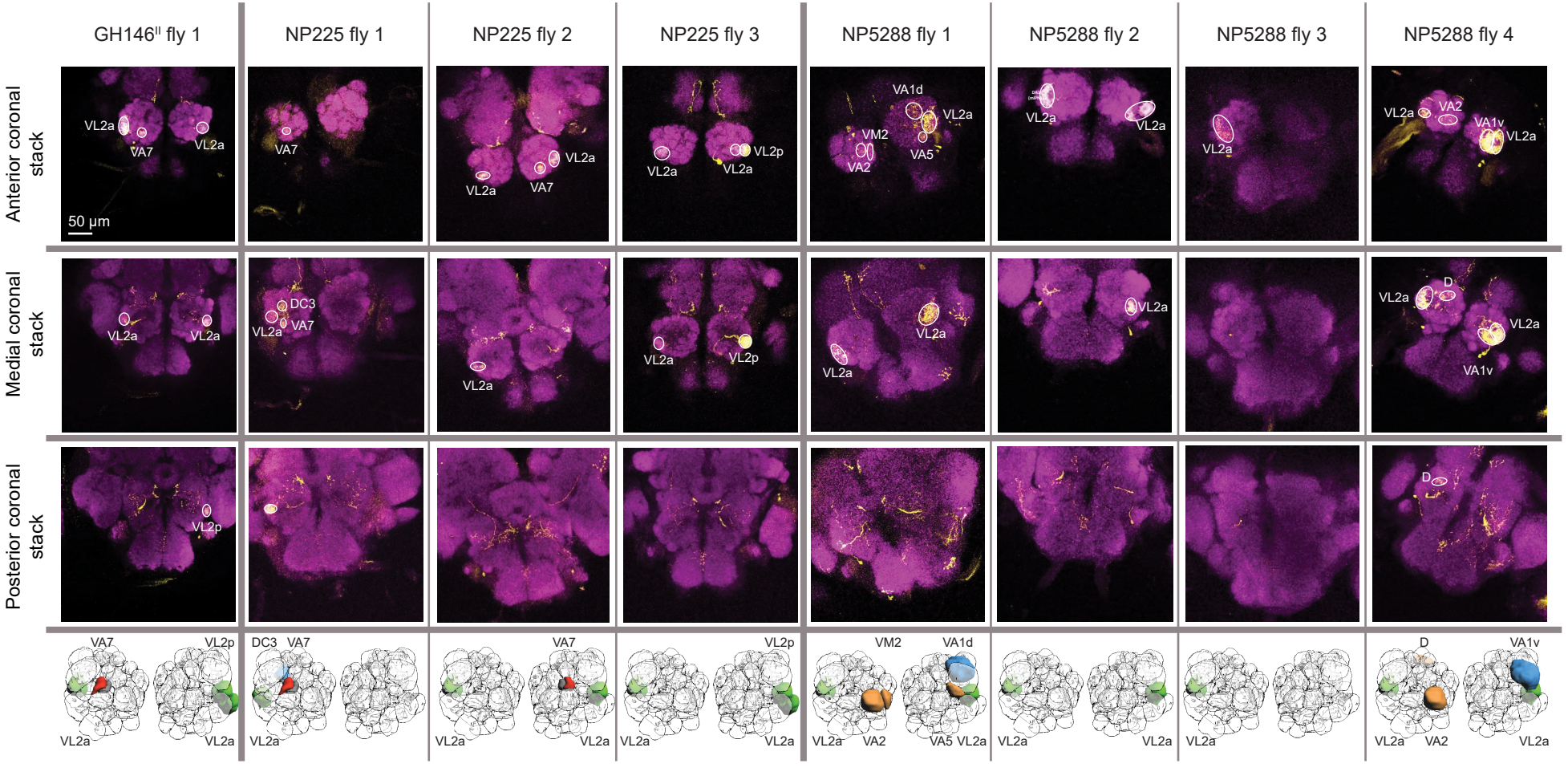
GH146II fly 1
NP225 fly 1
NP225 fly 2
NP225 fly 3
NP5288 fly 1
NP5288 fly 2
NP5288 fly 3
NP5288 fly 4
Anterior coronal stack
Medial coronal stack
Posterior coronal stack
50 µm
VL2a
VA7
VL2p
DC3
VA1d
VM2
VA2
VA5
VA1v
D

Figure S4: AL glomeruli labeled by subtracting GH146-QF from GH146^{II}-, NP225- and NP5288-GAL4. Related to Figure 6

Top, AL expression patterns when GH146^{II}-, NP225-, or NP5288-GAL4 driving CsChrimson.mVenus were intersected with GH146-QF driving the GAL4 inhibitor QUAS-GAL80 in individual flies. Maximum intensity projections of ~20 confocal sections (1 µm) through anterior, medial and posterior coronal stacks of the AL are presented. Only a small and relatively consistent subset of AL glomeruli is labeled across different flies. *Bottom*, schematic 3D illustrations[S2] of the spatial locations of the AL labeled glomeruli.

Variable	Parameter	Estimate	Standard error	|t|	p
Intercept	β0	2.108	1.007	2.094	0.0396
LH Commissural	β1	-0.01444	0.8336	0.01732	0.9862
APL	β2	-0.07926	1.026	0.07726	0.9386
Multiglomerular PN	β3	-0.5308	0.8372	0.6340	0.5280
Posterior LH	β4	-0.2355	0.8887	0.2650	0.7917
Anterior LH	β5	0.3569	0.8198	0.4354	0.6645
Medial SEZ	β6	-1.312	0.9052	1.449	0.1514
Lateral anterior SEZ	β7	-0.8764	1.339	0.6547	0.5147
Lateral posterior SEZ 1	β8	0.6457	1.195	0.5404	0.5905
Lateral posterior SEZ 2 (MooSEZ)	β9	8.378	0.8227	10.18	<0.0001

$$y \sim \beta_0 + \beta_1 X_1 + \beta_2 X_2 + \beta_3 X_3 + \beta_4 X_4 + \beta_5 X_5 + \beta_6 X_6 + \beta_7 X_7 + \beta_8 X_8 + \beta_9 X_9$$

Table S2: Multiple linear regression analysis for stochastic activation via the SPARC genetic method. Related to Figure 5.

Nine explanatory variables representing nine stochastically labeled neuronal clusters in GH146^{II}-GAL4 were used to predict average backward walking covered by single flies (n=85). Y denotes the dependent variable, β_0 denotes the y-intercept and β_n denotes the slope of the X_n independent variable. R^2 = 0.6311, adjusted R^2 = 0.5868, F(9, 75)=14.26, **** p<0.0001.

Supplemental References

S1. Lerner, H., Rozenfeld, E., Rozenman, B., Huetteroth, W., and Parnas, M. (2020). Differential Role for a Defined Lateral Horn Neuron Subset in Naïve Odor Valence in Drosophila. Sci. Rep.

S2. Grabe, V., Strutz, A., Baschwitz, A., Hansson, B.S., and Sachse, S. (2015). Digital in vivo 3D atlas of the antennal lobe of Drosophila melanogaster. J. Comp. Neurol.